Bending Rules in Graphene Kirigami

Bastien F. Grosso[1,3] and E. J. Mele[2,3,*]
[1]Institute of Theoretical Physics Ecole Polytechnique Federale de Lausanne (EPFL), Lausanne CH-1015, Switzerland
[2]Department of Physics and Astronomy University of Pennsylvania, Philadelphia, Pennsylvania 19104, USA
[3]Department of Physics Loughborough University, Loughborough LE11 3TU, United Kingdom
(Received 1 July 2015; published 4 November 2015)

The three-dimensional shapes of graphene sheets produced by nanoscale cut-and-join kirigami are studied by combining large-scale atomistic simulations with continuum elastic modeling. Lattice segments are selectively removed from a graphene sheet, and the structure is allowed to close by relaxing in the third dimension. The surface relaxation is limited by a nonzero bending modulus which produces a smoothly modulated landscape instead of the ridge-and-plateau motif found in macroscopic lattice kirigami. The resulting surface shapes and their interactions are well described by a new set of microscopic kirigami rules that resolve the competition between bending and stretching energies.

DOI: 10.1103/PhysRevLett.115.195501 PACS numbers: 61.48.Gh, 46.70.Hg, 61.72.-y

Bending and folding lifts a two-dimensional material into the third dimension and enables different physical functionalities. In a familiar example, folds can be introduced into a piece of paper to change its three-dimensional shape with or without allowing for tears. A lattice model for the former case (kirigami) has been studied recently [1] demonstrating rules for generating three-dimensional shapes by selective removal of segments from a parent honeycomb lattice and rejoining the holes by sharp folds. Because the folding rules so defined are essentially geometrical, it is possible that they could find applications in two-dimensional nanoscale materials and possibly even affect their electronic behavior [2].

However, applications to nanomaterials generally violate the two central tenets of macroscopic lattice kirigami: (a) the bending modulus is nonzero, prohibiting the formation of sharply folded edges, and (b) the system is compressible allowing it to store energy in shear and compressive strains. As a consequence, nanokirigami introduces a new family of three-dimensional deformations: the regular faceted structures of macroscopic lattice kirigami inevitably relax to softly rolling landscapes evocative of the English countryside. In this Letter, we study this problem for the prototypical case of graphene sheets embedding various forms of lattice kirigami and analyze their three-dimensional shapes by combining large-scale atomistic modeling [3,4] and analysis using long wavelength elastic theory [5–7]. The competition between bend and strain energies poses a challenging minimization problem for these systems, which we find is resolved through a compact set of bending rules. These rules, which are completely absent from the macroscopic variant of this problem, are essential at the nanoscale and generalize to a wide family of two-dimensional nanomaterials guiding the controlled design of desired strain and curvature fields with a microscopic cut-and-join motif.

Figure 2 compares the out-of-plane deflections of graphene disks that embed two elementary kirigami primitives. The top panel illustrates the procedure for generating these structures: all the models embed defects in which atoms are initially removed from a strip [Fig. 1(a)] that terminates on a dislocation with nearest-neighbor five- and seven-membered rings [Fig. 1(b)]. Figures 1(c) and 1(d) illustrate the relaxation of a (macroscopic) incompressible model that allows only for sharp folds. The atoms are reconnected along the dashed line of length d terminating on dislocations. Under these conditions, removal of the hole forces the sheet into the third dimensions via perpendicular creases that vertically displace the left- and right-hand regions in the same [Fig. 1(c)] or opposite [Fig. 1(d)] directions. The defect energy in these structures is confined to the creases so that the "up-up" (uu) and "up-down" (ud) patterns are degenerate [1]. Starting from these structures, we minimized the structural energy of an atomistic model using interaction potentials for carbon developed by Los and Fasolino (LF) [3,4] which allow bonds to rupture and reform and provide a reasonable description of the elastic properties for carbon materials in diverse bonding environments. The structures we develop should be distinguished from patterned graphenes retaining large open perforations designed to allow reversible large amplitude deformations under mechanical loading [8,9]. They are more akin to the fully bonded defect structures exhibiting height modulations found on scars that terminate on dislocation cores found in some single layer graphenes produced by chemical vapor deposition [10]. Two generic features of the fully relaxed structures are apparent in the lower panels of Figs. 1(e) and 1(f). For both defects, we find a smooth variation in elevation that persists into the far field with soft pleats sourced by their near-field defect structures. In the following, we are concerned with the far-field deflection patterns and examine structural models

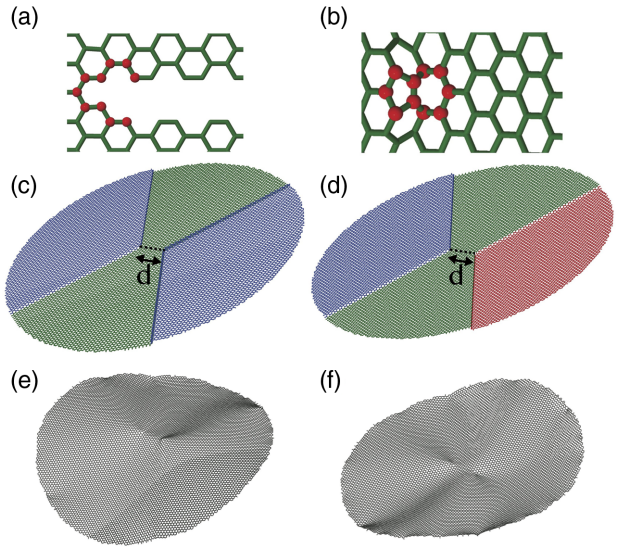

FIG. 1 (color online). Relaxation of a graphene kirigami in which atoms are removed from a finite strip of a flat graphene sheet (a), and the atoms are rejoined along a line terminating on nearest-neighbor pairs of five to seven disclinations (b). In (c) and (d), this structure is folded into the third dimension following the rules for macroscopic lattice kirigami. The atoms are rejoined along the dashed line, inducing sharp creases that separate plateaus that are displaced out of the plane in the same direction *uu* (c) or in opposite directions *ud* (d). These structures (c) and (d) relax to the shapes (e) and (f) generating a softly pleated landscape. The results are for an initial disk radius $R = 11.3$ nm, with $d = 1.86$ nm (panels c and e) and $d = 1.87$ nm (panels d and f).

with open boundary conditions and with vertex separation d much smaller than the lateral system size.

We quantify our observations by decomposing the height field $h(\mathbf{r})$ on a disk of radius R into angular harmonics

$$h(\mathbf{r}) = \sum_m h_m(r) e^{im\phi}. \tag{1}$$

Figure 2(a) shows the radial dependence $h_m(r)$ for the allowed even m amplitudes in the shape in Fig. 1(e). The relaxed structure is smooth, suppressing weight in its large m modes and confining its amplitude to the $m = 0, \pm 2$ deformations of the disk where $h_2(r)$ [Fig. 2(b)] is an increasing function of r out to the boundary. The bending energy has an areal energy density $u_b = \kappa_b(\nabla^2 h)^2/2$, and it is extremized by solutions of the biharmonic equation $\nabla^4 h = 0$. We find that the radial dependences of our relaxed structures $h_m(r)$ are well described by linear combinations of these bend optimized solutions projected into each angular harmonic subspace. For example, in the $m = 2$ subspace, the representation

$$h_2(r) = h_{-2}(r) = a_2 + \frac{b_2}{r^2} + c_2 r^2 + d_2 r^4 \tag{2}$$

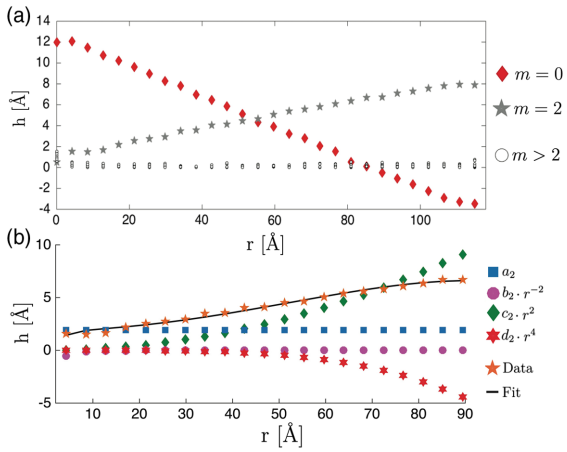

FIG. 2 (color online). (a) The height field for the relaxed *uu* structure of Fig. 1(e) is decomposed into its angular harmonics showing the radial dependence $h_m(r)$ with dominant contributions from $m = 0, \pm 2$. (b) The $m = 2$ radial dependence is well described by superposition of four solutions of a biharmonic equation projected into the $m = 2$ subspace. The profile contains two growing solutions with opposite signs which dominate the deflection in the far field.

describes the shape as shown in Fig. 2(b). Truncating the expansion (1) to include only the $m = 0$ and $m = \pm 2$ solutions provides an excellent reconstruction of the exact shape as demonstrated in Fig. 3(a). The *ud* structure [Fig. 1(f)] similarly relaxes to a smooth landscape well described by a superposition $m = \pm 1, \pm 3$ angular harmonics.

Note that the biharmonic equation admits *two* solutions that grow in the far field, and generically these are both present in the relaxed structures but they always appear

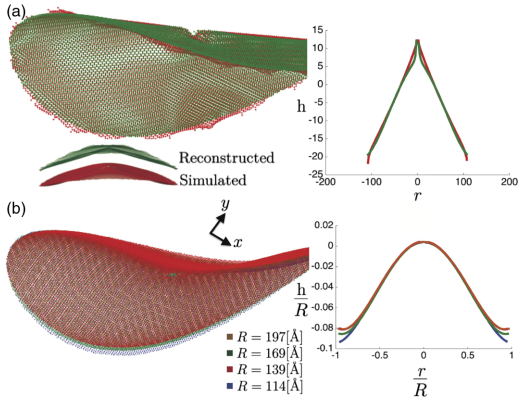

FIG. 3 (color online). (a) Reconstruction of the *uu* surface retaining only the $m = 0, \pm 2$ angular harmonics in the height field. The left side shows a superposition of the exact and reconstructed surfaces; the right inset gives a line plot along a coordinate that bisects the two dislocations that define the kirigami cut. Results are given for $R = 12.7$ nm and $d = 0.15$ nm. (b) Numerical test of the scaling rule Eq. (5) for the four different disk radii shown.

with opposite signs. Although it is tempting to attribute this to a boundary condition enforced at the edge of the disk, we find instead that this can be more easily understood as a global constraint on the shape. The growing solutions must compete in order to avoid a large strain energy penalty induced by their (locally) nonzero Gaussian curvatures. Note that a linear combination of the growing solutions in Eq. (2) makes a contribution to the Gaussian curvature that is *bilinear* in the expansion coefficients for h_2; explicitly, in the far field, we have for the determinant of the curvature tensor

$$\mathcal{C}_2^{>} = -4[c_2^2 + 6c_2 d_2 r^2 + 9d_2^2 r^4 \sin^2(2\phi)]. \tag{3}$$

Following Nelson and Peliti [6], we recall that a coupling of the local Gaussian curvature to in-plane strain mediates nonlocal ultra-long-range interactions between remote Gaussian curvatures diverging in Fourier space $\propto q^{-4}$. Consequently, for a large system under open boundary conditions we can avoid a macroscopic energy that grows faster than the system size if its integrated Gaussian curvature vanishes. In the space of m-projected biharmonic solutions, the residual Gaussian curvature cannot be made to vanish everywhere, and with zero mean the residual curvature can be usefully described by its nonvanishing moments. For $m = 2$ and using Eq. (3), we find that the disk-integrated curvature vanishes if the boundary ratio $\nu = d_2 R^2/c_2 = -0.423$, in good agreement with the ratio (~ -0.47) obtained from the numerical calculations. We carried out similar analysis for different structures and in various angular momentum channels m in the expansion (1) and find that the boundary ratio is m dependent and consistent with our simulation data.

The surfaces shown in Figs. 1(e) and 1(f) are, therefore, determined by three rules that resolve the competition between its bending and stretching energy in the elastically stiff (weakly compressible) limit: (1) the height field smooths by relaxing its amplitude to its low-order symmetry-allowed angular harmonics, (2) the radial dependence in each m channel superposes biharmonic bend optimized solutions, and (3) these appear in "well-tempered" combinations that also avoid a large strain energy penalty by quenching the *integrated* Gaussian curvature. The defect energy is then determined by the core energy of the terminal dislocations, the bending energy in the extremal solution, and the strain energy imposed by its residual Gaussian curvature.

The argument given above fixes the amplitude ratio of the far-field growing solutions but not their overall magnitudes which determine the degree of "warping" of the kirigamied disk. A scaling argument reveals that the latter is determined by the boundary energy on the perimeter of the disk, presumably arising from the inequivalence of bulk (area) and surface (perimeter) interactions. For example, a structure with $c_2 \neq 0$ that results from a boundary interaction proportional to R and is opposed by a bulk interaction proportional to R^2 is described by an energy function

$$U = \alpha R^2 c_2^2 + \beta R c_2, \tag{4}$$

where $\alpha > 0$ and β are constants, giving $\bar{c}_2 = -\beta/2\alpha R$. We can express the growing solutions of Eq. (2) in a scaling form

$$\frac{h_2^{>}}{R} = \frac{-\beta}{2\alpha}\left[\left(\frac{r}{R}\right)^2 + \nu\left(\frac{r}{R}\right)^4\right]. \tag{5}$$

Thus, for $m = 2$, by expressing all lengths (h, r) in units of the disk radius R, one obtains a universal warped shape determined by the value of β. Note that this scaling rule is m dependent; i.e., different m's all show scaling but are described by different scaling functions. The full shape is scalable to the extent that it can be described by a single dominant angular harmonic. In Fig. 3(b), we test this hypothesis by plotting the scaled height $h' = h_2^{>}/R$ versus the scaled radial coordinate $r' = r/R$ demonstrating its near collapse to a single profile. We conclude that an unwarped kirigami profile with no growing solutions is nongeneric and would require fine-tuning the system to a special point at $\beta = 0$. This is evidently not a property of the LF potentials for carbon [4] or of any generic model for the interparticle interactions. Therefore, the kirigamied disks generally feature a long-distance shape modulation that cannot be confined to the defect. We interpret this as the microscopic analog to the step risers in macroscopic lattice kirigami that also propagate to the sample boundaries and connect the core defect structure with the edge. It also suggests the possibility of tuning the shape of our nanoscale variant by functionalizing the boundaries to control the edge potential parameter β.

These considerations can also be used to understand the energetics of microscopic kirigami. In macroscopic lattice kirigami, the edges are sharp and the *uu* structure [Fig. 1(c)] is degenerate in energy with the *ud* structure [Fig. 1(d)]. Furthermore (ignoring finite size effects from the termination of creases at the outer edges), the energy of a *uu* configuration is independent of the separation (d) of the dislocations that define the vertices of their plateaus [Figs. 1(c) and 1(d)] since the sharp steps are nonoverlapping. These features do not apply to microscopic kirigami where the height profile is smooth and the dislocations can interact via overlap of their induced curvature fields. In Fig. 4, we compare the energies of the *uu* and *ud* configurations as a function of the vertex separation d. (To obtain these data, the relaxation calculations were carried out on square rather than circular models so that the number of atoms is the same in each sampled structure.) The *uu* configuration is energetically preferred for any intervertex spacing d. At intermediate separations, the

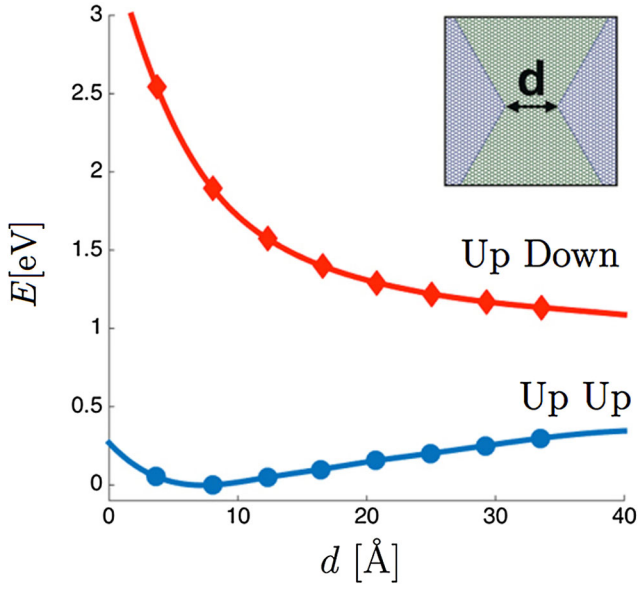

FIG. 4 (color online). Energies for graphene kirigami as a function of vertex separation d on a square sample with initial width $L = 22.4$ nm (inset). Energies are plotted relative to the minimum energy of the uu configuration. The uu and ud configurations are nondegenerate and the bend-induced ud potential is repulsive. These properties are described qualitatively by continuum elastic theory where the energy differences and their dependence on d are determined mainly by the mean curvature fields in the relaxed structures.

energy degeneracy is, in fact, strongly broken; for example, the energy difference for a separation of ~20 Å is ≈1.0 eV.

By analyzing these structures within continuum elastic theory, we conclude that these energy differences arise from interactions that are mediated nearly entirely by the mean curvature of the extended overlapping height fields. The stretching energy, while present is nearly independent of d, indicating that its role is to simply renormalize the self-energies in these structures. The interactions between defects mediated by the bending energy then lead qualitatively to the interaction profile shown in Fig. 4. This behavior is captured even in a lowest-order elastic theory. We first calculate the Lamé coefficients λ and μ and bending modulus κ_b using our model potential giving the values presented in Table I.

In this expansion, the energy can be partitioned into a pure bending contribution

$$U_b = \frac{\kappa_b}{2} \int d^2\mathbf{r} (\nabla^2 h)^2 \tag{6}$$

and a strain term

$$U_s = \frac{1}{2} \int d^2\mathbf{r} (2\mu u_{ij}^2 + \lambda u_{kk}^2), \tag{7}$$

TABLE I. Two-dimensional Lamé coefficients, bulk modulus, and bending modulus obtained by fitting the structural energies for deformed graphene sheets using the interatomic potentials of Los and Fasolino [4].

Elastic constant	Fitted value
λ	3.03 eV/Å^2
μ	10.67 eV/Å^2
B	13.7 eV/Å^2
κ_b	0.70 eV

where u_{ij} are the linearized strains $(\partial_i u_j + \partial_j u_i)/2$. [We have investigated the role of the nonlinear strain terms that can appear, Eq. (7), and find that they do not qualitatively change our conclusions.] Although the contribution from U_s can be formally eliminated in favor of a (strongly) nonlocal interaction between Gaussian curvatures [6], we choose instead to simply calculate the energy using the formula Eq. (7).

In the continuum model, one finds that energy degeneracy of the uu and ud geometries is resolved and the uu configuration always favored. This can be understood if one regards the height fields of the two defects as additive. In the uu configuration, the height deformations appear with opposite signs and nearly cancel in the far field, while in the ud configuration they interfere constructively. The bending energy (though not the Gaussian curvature-induced stretching energy) is quadratic in derivatives of h, and so the relative sign of the superposed height fields determines the sign of their interaction. This predicts that the uu structure has lower energy and favors small d where the cancellation is more nearly complete (the upturn at small d in Fig. 4 manifests the nonadditivity of the short-range deflection fields). Conversely, the height fields in the ud structure never compensate and favor large d just as seen in the lattice calculation. This behavior captures the essential results of the full atomistic calculations (Fig. 4), but it fails to quantitatively account for their magnitudes, as can be expected since these structures are actually highly strained. We also note that our fitted bending modulus in Table I ($\kappa_b = 0.70$ eV) is in reasonable agreement with values (~0.82 eV) previously reported studying bending energies of graphene sheets using similar empirical potentials [11,12]. The microscopic origin of this bare bending modulus is discussed in Ref. [12], suggesting that quantum mechanical models yield a modulus approximately a factor of 2 larger. Furthermore, the bending modulus is both predicted [11] and observed [9] to be renormalized upward by thermal fluctuations in two-dimensional membranes [11]. All these trends further support our conclusion that bend-optimized shapes will be realized in graphene kirigami.

Insights from the bending energetics of nanoscale kirigami may be useful for stabilizing structures in macroscopic kirigami. The degeneracy of the uu and ud motifs is

problematic for applications that would seek to stabilize a single target shape. This can be resolved by the introduction of macroscopic couplings that introduce an effective bending rigidity. Braces that suppress or promote bending can be engineered to introduce nonlocal coupling between neighboring step risers and provide a route to encoding a unique surface structure.

The analytic structure of our graphene-kirigami solutions also has important consequences for its Dirac electronic structure near charge neutrality. In these structures, topological defects in their bond networks induce surface deformations with bend and (locally) nonzero Gaussian curvature. Separately, these structural features all couple to electronic motion in the tangent plane [13–17] where the natural language for this coupling involves valley asymmetric bend- and strain-induced gauge fields [16]. The gauge fields induced by pure bending are curl-free and have the innocuous effect of simply shifting the Dirac points in momentum space. By contrast, Gaussian curvature is topologically nontrivial and links the system with a (valley-dependent) local flux [15]. The essential characteristic of the m-projected solutions presented above is that a competition between bending and stretching energies generates a landscape where the Gaussian curvature is globally compensated (so that the total pseudoflux is zero), but this can only be accomplished by sign changes on a network of nodal lines that carry the signature of the fully relaxed kirigami. The possibility of confining electronic modes along these lines and their role in defining the low-energy spectral and transport properties now presents an important problem for further study.

This work was supported by the Department of Energy under Grant No. DE FG02-84ER45118. E. J. M. acknowledges support from the Leverhulme Trust at Loughborough University where this work was carried out.

*mele@physics.upenn.edu

[1] T. Castle, Y. Cho, X. Gong, E. Jung, D. M. Sussman, S. Yang, and R. D. Kamien, Phys. Rev. Lett. **113**, 245502 (2014).
[2] O. V. Yazyev and Y. P. Chen, Nat. Nanotechnol. **9**, 755 (2014).
[3] S. Plimpton, J. Comp. Physiol. **117**, 1 (1995).
[4] J. H. Los and A. Fasolino, Phys. Rev. B **68**, 024107 (2003).
[5] L. D. Landau and E. M. Lifshitz, *Theory of Elasticity* (Pergamon, New York, 1970).
[6] D. R. Nelson and L. Peliti, J. Phys. (Paris) **48**, 1085 (1987).
[7] H. S. Seung and D. R. Nelson, Phys. Rev. A **38**, 1005 (1988).
[8] Z. Qi, D. K. Campbell, and H. S. Park, Phys. Rev. B **90**, 245437 (2014).
[9] M. K. Blees, A. W. Barnard, P. A. Rose, S. P. Roberts, K. L. McGill, P. Y. Huang, A. R. Ruyack, J. W. Kevek, B. Kobrin, D. A. Muller, and P. L. McEuen, Nature (London) **524**, 204 (2015).
[10] O. Lehtinen, S. Kurasch, A. V. Krasheninnikov, and U. Kaiser, Nat. Commun. **4**, 2098 (2013).
[11] A Fasolino, J. H. Los, and M. I. Katsnelson, Nature (London) **6**, 858 (2007).
[12] I. Nikiforov, E. Dontsova, R. D. James, and T. Dumitrică, Phys. Rev. B **89**, 155437 (2014).
[13] C. L. Kane and E. J. Mele, Phys. Rev. Lett. **78**, 1932 (1997).
[14] A. Mesaros, D. Sadri, and J. Zaanen, Phys. Rev. B **79**, 155111 (2009).
[15] T. O. Wehling, A. V. Balatsky, A. M. Tsvelik, M. I. Katsnelson, and A. I. Lichtenstein, Europhys. Lett. **84**, 17003 (2008).
[16] F. Guinea, M. I. Katsnelson, and A. K. Geim, Nat. Phys. **6**, 30 (2010).
[17] M. Phillips and E. J. Mele, Phys. Rev. B **91**, 125404 (2015).